ATRA and ATO at 50% doses. Whilst the benefit of prophylactic corticosteroids in prevention of DS is uncertain and mainly reserved for patients presenting with a white cell count >5 × 10^9/l, we used prophylactic low dose dexamethasone.[9]

Although haemorrhagic complications of APML predominate and are reduced by ATRA, thrombosis is not uncommon; however, this risk is not reduced by ATRA.[1,2] The acute inflammatory state in COVID-19, in addition to the known thrombotic risk of hospitalisation, results in a highly pro-thrombotic state. This, when combined with APML thrombotic complications were felt to warrant intermediate dose enoxaparin prophylaxis in our case.

This case presented challenges due to atypical coagulation studies in the context of COVID-19. Laboratory findings of APML can be disguised in the context of COVID-19, thus stressing the need to suspect a potential acute leukaemia in COVID-19 presenting with neutropenia. The complexities of balancing risk of DS on the background of already severely inflamed lungs and the risk/benefit of prophylaxis with steroids made it necessary to consider treatment alterations.

Isabel Farmer[1,†]
Jumoke Okikiolu[1,†]
Matthew Steel[1]
Chandima Wanniarachchi[1]
Shona Littlewood[1]
Sunil Gupta[1]
Muragaiyan Thanigaikumar[1]
S. Helen Oram[1]
Mufaddal Moonim[2]
Austin G. Kulasekararaj[3]
Tullie Yeghen[1]

[1]*Department of Haematology, Lewisham and Greenwich NHS Trust,* [2]*Department of Histopathology, Guys and St Thomas NHS Foundation Trust and* [3]*Department of Haematological Medicine, King's College Hospital, London, UK.*
E-mail: isabelfarmer@nhs.net

[†]Joint first authors.

Keywords: acute promyelocytic leukaemia, coagulation, clinical haematology, differentiation

First published online 8 June 2020
doi: 10.1111/bjh.16864

References

1. Breen KA, Grimwade D, Hunt BJ. The pathogenesis and management of the coagulopathy of acute promyelocytic leukaemia. *Br J Haematol*. 2012;**156**:24–36.
2. David S, Mathews V. Mechanisms and management of coagulopathy in acute promyelocytic leukemia. *Thromb Res*. 2018;**164**:S82–S88.
3. Connors J, States U, Levy J, States U. COVID-19 and its implications for thrombosis and anticoagulation. *Blood*. 2020. https://doi.org/10.1182/blood.2020006000.
4. Thachil J, Tang N, Gando S, Falanga A, Cattaneo M, Levi M, et al. ISTH interim guidance on recognition and management of coagulopathy in COVID-19. *J Thromb Haemost*. 2020;**18**(5):1023–6.
5. Tang N, Li D, Wang X, Sun Z. Abnormal coagulation parameters are associated with poor prognosis in patients with novel coronavirus pneumonia. *J Thromb Haemost*. 2020;**18**(4):844–7.
6. Tan L, Wang Q, Zhang D, Ding J, Huang Q, Tang YQ, et al. Lymphopenia predicts disease severity of COVID-19: a descriptive and predictive study. *Signal Transduct Target Ther*. 2020;**5**:16–8.
7. Rego EM, De Santis GC. Differentiation syndrome in promyelocytic leukemia: clinical presentation, pathogenesis and treatment. *Mediterr J Hematol Infect Dis*. 2011;**3**:e2011048. https://doi.org/10.4084/MJHID.2011.048.
8. Sentero D, Hosenpud J. Retinoic acid syndrome in acute promyelocytic leukemia. *Wisconsin Med J*. 1997;**96**:35–8.
9. Sanz MA, Fenaux P, Tallman MS, Estey EH, Löwenberg B, Naoe T, et al. Management of acute promyelocytic leukemia: updated recommendations from an expert panel of the European LeukemiaNet. *Blood*. 2019;**133**:1630–43.

Rapid diagnosis of hereditary haemolytic anaemias using automated rheoscopy and supervised machine learning

Haemolytic anaemias arise when red blood cell (RBC) integrity is compromised, eventually resulting in premature clearance or lysis and leading to anaemia when these effects cannot be sufficiently compensated by the capacity of the bone marrow to produce new cells.[1] Hereditary anaemia occurs as a consequence of genetic mutation[2] (e.g. affecting membrane complex or cytoskeletal proteins, haemoglobin or metabolic enzymes), and diagnosing affected patients is a complex process since, given the wide variety of possible genetic causes, multiple examinations must be performed and an unambiguous result is usually reached only after DNA sequencing.[3] Furthermore, phenotypic severity can vary widely not just among individuals with different mutations but also among individuals suffering from the same mutation, thereby complicating diagnosis.[4]

While molecular diagnoses have become increasingly easier, cheaper and faster to perform in recent years, constraints on their use still exist,[5] and phenotype-based diagnostic methods still constitute an important proposition.

Ektacytometry is a standard diagnostic platform for RBC disorders[6,7] but only provides cell population-based data and requires a trained expert for data interpretation. Single-cell rheoscopy can provide additional information, with higher complexity as a drawback; however, analysis of such data could potentially be facilitated by the use of machine learning (ML, automated, algorithm-based systems that generate data-driven predictions[8]).

We present here a preliminary framework for automated rheoscopy-based diagnosis of several types of hereditary haemolytic anaemia samples **Fig 1A** that requires low sample volumes and is efficient, rapid and expandable.

Materials and methods

Peripheral blood donor and patient samples

Healthy control donor and diagnosed patient samples were collected according to procedures approved by the research ethics committee and in accordance with the Declaration of Helsinki. In all, 47 blood samples were analysed at the University of Bristol (United Kingdom) following shipment from clinics in Milan (Italy) or Utrecht (the Netherlands) [6 controls, 13 hereditary spherocytosis (HS) patients, 9 congenital dyserythropoietic anaemia type II (CDAII) patients, 6

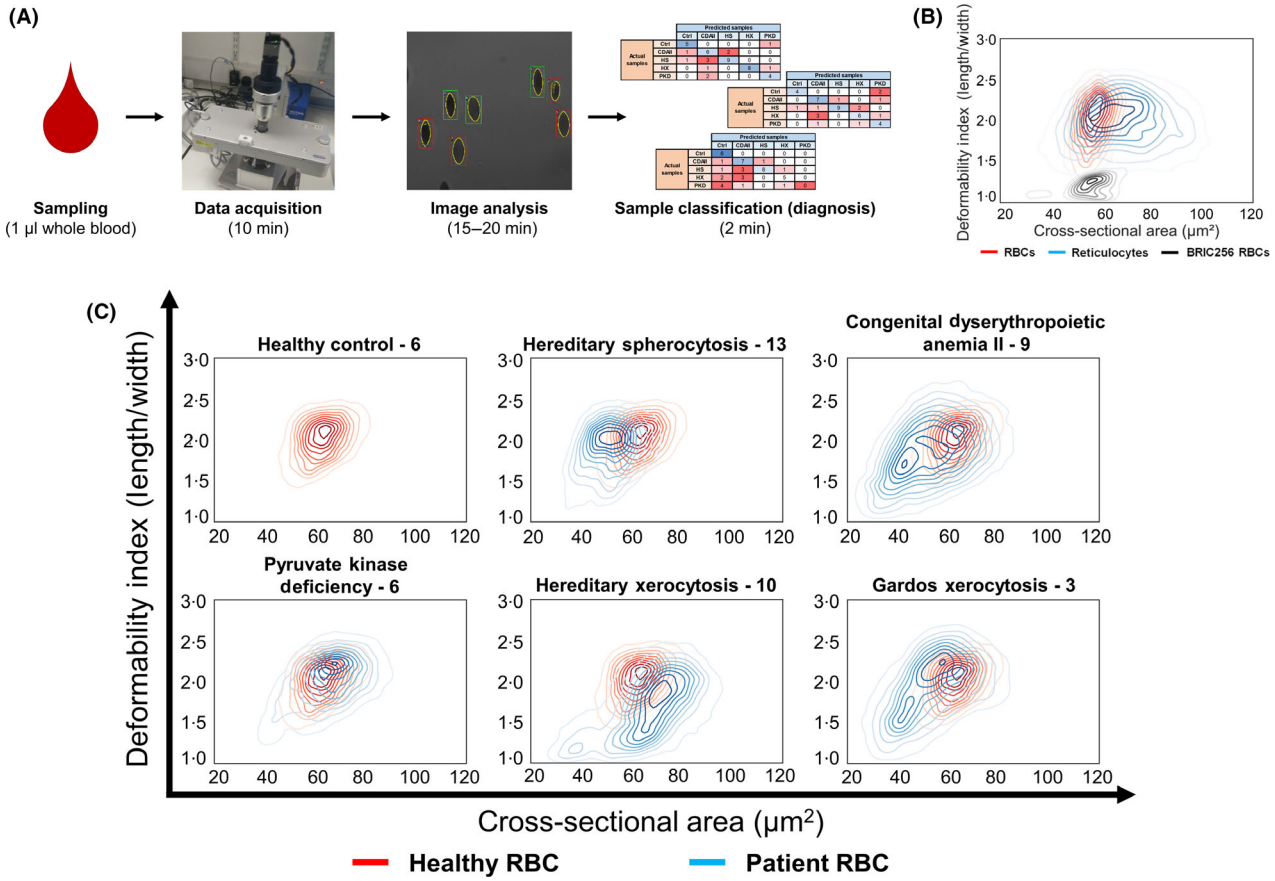

Fig 1. Different hereditary rare anaemias display distinct area and deformability profiles. (A) Design of the method for automatic sample classification. Whole blood is collected by the clinician, and a sample is obtained and processed using an Automated Rheoscope and Cell Analyzer (ARCA). Images acquired are subjected to computational analysis to determine cross-sectional area and deformability of at least 1000 individual cells, and the resulting datasets are then classified through trained computational models, achieving a diagnosis in less than 30 min. **(B)** Contour plots of cross-sectional area plotted against the deformability index (as measured by dividing cell length by cell width), visualizing the probability distribution of erythrocytes (RBCs), cultured reticulocytes (reticulocytes) and erythrocytes treated with an anti-Glycophorin A antibody (BRIC256, International Blood Group Reference Laboratory) before analysis to induce membrane stiffening (BRIC256 RBCs). The control erythrocyte and cultured reticulocyte data shown in this panel were previously reported in Moura et al.9 A minimum of 1000 cells were analysed per sample. All samples were analysed using the ARCA. (C) Contour plots of cross-sectional area plotted against the deformability index (as measured by dividing cell length by cell width), visualizing the probability distribution of patient samples overlaid to allow for comparison with healthy controls. A minimum of 1000 cells were analysed per blood sample. All samples were analysed using the ARCA. The samples are listed from left to right: Top row: healthy controls (n = 6), hereditary spherocytosis patients (n = 13), congenital dyserythropoietic anaemia II patients (n = 9). Bottom row: pyruvate kinase deficiency patients (n = 6), dehydrated stomatocytosis type 1 or hereditary xerocytosis patients (n = 10), dehydrated stomatocytosis type 2 or Gardos xerocytosis patients (n = 3).

pyruvate kinase deficiency (PKD) patients, 10 hereditary xerocytosis/ dehydrated hereditary stomatocytosis (DHS) 1 (HX) patients and 3 Gardos xerocytosis/ DHS2 (GX) patients]. A further 26 samples (11 controls, 7 HS patients and 8 hereditary elliptocytosis [HE] patients) were analysed at Sanquin (Amsterdam, the Netherlands).

Automated Rheoscope and Cell Analyser

An amount of 1 μl of whole blood was diluted in 200 μl of a polyvinylpyrrolidone solution (viscosity 28·1 mPa·s). Samples were assessed in an Automated Rheoscope and Cell Analyser (ARCA) according to published protocols.[9] At least 1000 cells per sample were analysed, providing the deformability index (DI) and cross-sectional area (area) quantification.

Computational analysis

A Python script was developed for statistical analysis, data visualisation and automatic dataset classification (Data availability). The full datasets used for training purposes were sampled and randomised into testing (500 cells) and training datasets (remainder). Deformability Index (DI) and area were normalised by the maximum measurable values (3.3/5.0 DI from Bristol and Sanquin, respectively, and 140 μm^2 area) and the training datasets were repeatedly subjected to random sampling to generate 10,000 subsets of 500 cells each, followed by calculation of the average and standard deviation of the DI and area. Each sample category was then attributed unique identifiers. Classifiers were generated with the scikit-learn package,[10] trained with the generated subsets and tested with the initial testing subsets. Classification of unseen datasets was performed by selecting the mode of the machine-selected identifiers after 10,000 classifications.

Results and discussion

We have demonstrated in previous work that automated rheoscopy-based analyses can elucidate differences arising from reticulocyte maturation[9] as well as loss of cellular stability.[11] A particularly interesting observation from the same work was the fact that combining the single-cell deformability index (DI) and cross-sectional area measurements provides a novel metric (Fig 1B) which to date has not been examined in the context of disease diagnosis.

Therefore, we evaluated whole blood samples from diagnosed anaemic patients of varied aetiologies (HS, CDAII, PKD, HX and GX) against healthy donors using the proposed methodology (Fig 1C). Crucially, despite these diseases being frequently misdiagnosed due to overlapping clinical or morphological phenotypes,[12,13] we observed them to display unique rheoscopy "fingerprints" upon visualisation.

Machine-learning algorithms were next explored to automate the classification of ARCA data and thus facilitate the processing of larger numbers of samples, A flow chart listing the procedure used for these attempts is displayed in Fig 2A.

To provide sufficient information for training a ML classifier, the data were augmented through random sampling, vastly extending the number of new datasets with similar characteristics. We then tested the trained classifiers on a combination of fully unseen data and the testing sets generated before augmentation. A full summary of the prediction accuracies achieved (and listing the best performing classifiers) is provided in Fig 2B with the best performing algorithm correctly identifying sample datasets with 92% accuracy (Fig 2C). We note that the GX samples were excluded due to the sample number being too low for classifier training.

For further verification, the classifiers were retrained on additional samples (11 controls, 7 HS patients and 8 HE patients) obtained on a second ARCA device in an independent laboratory and using different acquisition settings. Again, we observed increasing classification accuracy up to the use of six training datasets (at which point the classifier likely overfits these data), as per Fig 2D, achieving a final prediction accuracy for multiclass classification that is comparable to that offered by osmotic gradient ektacytometry when classifying HS samples alone.[14] Importantly, the best performing algorithms utilized here achieve complete differentiation between controls and diseased patients and accurately identify a variety of disorders potentially allowing for the rapid preliminary identification or discrimination of more elusive diseases[15] (such as CDAII and PKD) without time-consuming laboratory assays or molecular testing methods. Furthermore, the possibility to continuously incorporate data from new samples or the expansion with haematological conditions beyond those characterised in this study may ultimately allow for diagnosing a large number of samples in a relatively short period using minimal sample volumes. In conclusion, the method described in this work represents an exciting step forward towards facilitating the improved diagnosis of haemolytic anaemias.

Acknowledgements

The authors would like to thank the donors, patients and their family members for their willingness to participate in this research. The authors thank Mr. Ario Sadafi (Technische Universität München, Munich, Germany) for helpful discussions regarding feature extraction for machine-learning algorithm development.

Funding information

PLM was funded by the European Union (H2020-MSCAITN-2015, "RELEVANCE", Grant agreement number 675117). MAER is supported by Eurostars grant estar18105 and by an unrestricted grant provided by RR Mechatronics. PB was funded by the Fondazione IRCCS Ca' Granda

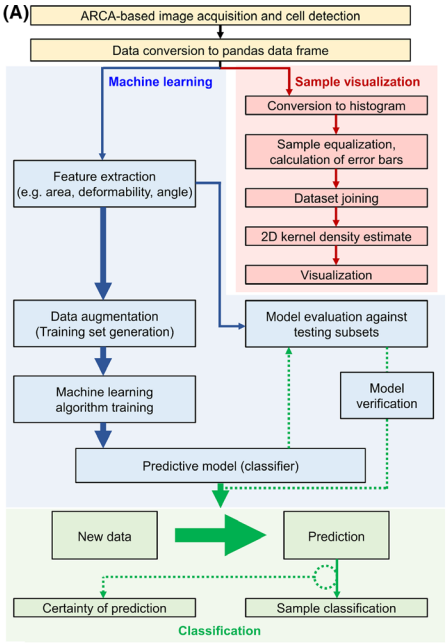

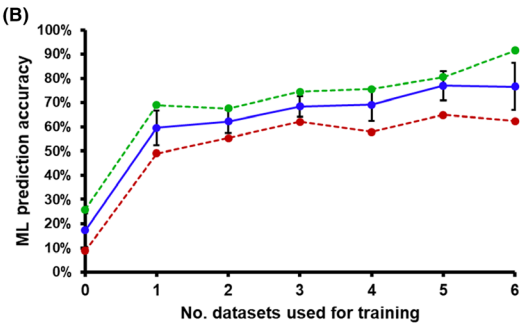

Prediction accuracy	No. datasets used for training						
	0	1	2	3	4	5	6
K-Nearest neighbours classifier	20·00%	62·34%	66·51%	69·85%	73·18%	79·85%	75·67%
Bagging classifier	**25·90%**	54·38%	61·40%	**74·55%**	**75·62%**	78·31%	**91·54%**
AdaBoost (SAMME)	20·00%	49·03%	64·02%	66·74%	57·86%	64·91%	62·36%
Multi-layer perceptron classifier	9·06%	**68·96%**	55·38%	70·35%	68·07%	80·07%	75·67%
Gradient boosting	20·00%	58·29%	**67·59%**	66·74%	73·40%	**80·53%**	81·94%
Random forests	8·87%	64·51%	58·26%	62·12%	66·31%	78·31%	72·34%
Minimum accuracy	8·87%	49·03%	55·38%	62·12%	57·86%	64·91%	62·36%
Average accuracy	17·30%	59·58%	62·19%	68·39%	69·07%	76·99%	76·59%
Standard deviation	6·85%	7·21%	4·77%	4·21%	6·52%	5·99%	9·74%
Maximum accuracy	25·90%	68·96%	67·59%	74·55%	75·62%	80·53%	91·54%

(C)

Bagging classifier

		Predicted samples						
		Ctrl	CDAII	HS	HX	PKD	Total	Acc
Actual samples	Ctrl	6	0	0	0	0	6	100%
	CDAII	0	9	0	0	0	9	100%
	HS	0	2	11	0	0	13	85%
	HX	0	0	1	9	0	10	90%
	PKD	0	0	0	0	6	6	100%
						Average accuracy		92%

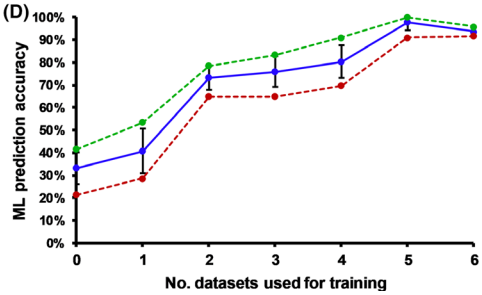

Fig 2. Machine-learning-based classification of automated rheoscopy datasets provides accurate diagnoses for unseen samples. (A) Flow diagram outlining the procedure for ARCA-based data visualisation and automated sample classification. The sample is first analysed to produce a raw data table. These data are then reorganised into a Python pandas ("panel data") data frame for ease of processing. If visualisation is required, samples from a given sample type are stochastically equalised in cell number, joined and subjected to kernel density estimation to estimate the probability density functions of analysed features (e.g. cross-sectional area, deformability index, cell angle) and then visualized through contour plots or scatter plots. Data to be used for machine learning undergo feature extraction (removal of all non-essential information) and a subsection is sampled randomly (without reposition) for creation of a testing set. The remaining data then undergo augmentation by generation of a series of randomly sampled datasets (with reposition, 10,000×) which will be used for training a supervised machine-learning algorithm. After training, a predictive model (i.e. classifier) is generated which first is tested with the previously generated testing set. Upon satisfactory results with the testing set, the classifier can then generate predictions for new unseen data. The final results consist of a sample label (or classification) and the certainty of that classification (B) Comparison of the overall prediction accuracy of multiple supervised machine-learning algorithms in ARCA-based automated sample diagnosis as a function of the number of datasets per condition used for classifier training (from no datasets used, which should result in a random diagnosis, to a maximum of six datasets), comparing the samples analysed at the University of Bristol (except Gardos xerocytosis samples, which were too few to analyse). Prediction accuracy is coloured on a percentage scale from red (0%) to blue (100%). The best-performing algorithm per no. of datasets is bolded in the accuracy matrix. The graph displays the average prediction accuracy of all algorithms (blue). Error bars = ± standard deviation (SD). The prediction accuracies of the best-performing algorithms are plotted in green, while the prediction accuracies of the worst-performing algorithms are plotted in red. (C) Prediction accuracy of the best performing algorithm in (B). The samples used consist of healthy controls, congenital dyserythropoietic anaemia II patients (CDAII), hereditary spherocytosis patients (HS), hereditary xerocytosis patients (HX) and pyruvate kinase deficiency patients (PKD). Rows identify real samples provided, whilst columns identify the algorithm's prediction of the provided samples' identity. The blue diagonal indicates samples that were correctly diagnosed (true positives). Red cells in the surrounding matrix indicate incorrect diagnoses (i.e. two HS samples were misdiagnosed as CDAII and one HX sample was misdiagnosed as HS). Accuracy is provided as a percentage of the true positives within the total number of samples and is coloured on a percentage scale from red (0%) to blue (100%). Average accuracy is provided as an average of the accuracies for all sample types. Data for all other algorithms and sample numbers tested are provided in Figs S1–S7. (D) Comparison of the overall prediction accuracy of multiple supervised machine-learning algorithms in ARCA-based automated sample diagnosis as a function of the number of datasets used for training, comparing samples from healthy controls, hereditary spherocytosis patients and hereditary elliptocytosis patients analysed at Sanquin. The graph displays the average prediction accuracy of all algorithms (blue). Error bars = ±SD. The prediction accuracies of the best-performing algorithms are plotted in green, while the prediction accuracies of the worst-performing algorithms are plotted in red.

Ospedale Maggiore Policlinico, Grant no. 2019 175/02, 2019. AMT and TJS were funded by an NHS Blood and Transplant (NHSBT) R&D grant (WP15-05) and the National Institute for Health Research Blood and Transplant Research Unit (NIHR BTRU) in Red Cell Products (IS-BTU-1214-10032). The views expressed are those of the author(s) and not necessarily those of the NIHR or the Department of Health and Social Care.

Author contributions

PLM acquired data, prepared figures and developed the Python code for dataset analysis and classification. JGGD and GJS provided essential ARCA equipment and image analysis software. MAER and RvW diagnosed HX patients and provided blood samples. MV and RvZ diagnosed HS and HE patients and performed initial ARCA analysis. EF and PB diagnosed HS, CDAII, HX and PKD patients and provided blood samples. PLM, AMT and TJS conceived and designed experiments and wrote the manuscript. TJS and AMT contributed equally to conception and supervision of the work. All authors read and edited the manuscript.

Conflicts of interest

The authors declare no competing financial interests.

Data Availability Statement

All raw ARCA datasets obtained during this study, Python scripts generated for dataset analysis, classifier training and sample classification and the confusion matrices generated for classifier evaluation have been made publicly available through the following Github repository: https://github.com/pedrolmoura/ARCA-ML.

Pedro L. Moura[1,2]
Johannes G. G. Dobbe[3]
Geert J. Streekstra[3]
Minke A. E. Rab[4,5]
Martijn Veldthuis[6]
Elisa Fermo[7]
Richard van Wijk[4]
Rob van Zwieten[6,8]
Paola Bianchi[7]
Ashley M. Toye[1,2,9,†]
Timothy J. Satchwell[1,2,9,†]

[1]School of Biochemistry, University of Bristol, Biomedical Sciences Building, University Walk, Bristol, BS8 1TD, UK, [2]NIHR Blood and Transplant Research Unit in Red Cell Products, University of Bristol, Bristol, UK, [3]Department of Biomedical Engineering and Physics, Amsterdam UMC, University of Amsterdam, Amsterdam, The Netherlands, [4]Department of Clinical Chemistry and Haematology, University Medical Center Utrecht, Utrecht University, Utrecht, The Netherlands, [5]Van Creveldkliniek, University Medical Center Utrecht, Utrecht University, Utrecht, The Netherlands, [6]Department of Blood Cell Research, Amsterdam, The Netherlands, [7]UOC Ematologia, UOS Fisiopatologia delle Anemie, Fondazione IRCCS Ca' Granda Ospedale Maggiore Policlinico, Milano, Italy, [8]Laboratory of Red Blood Cell Diagnostics, Amsterdam, The Netherlands and [9]Bristol Institute for Transfusion Sciences, National Health Service Blood and Transplant (NHSBT), Filton, UK.
E-mails: ash.m.toye@bristol.ac.uk; t.satchwell@bristol.ac.uk

Present address
Department of Medicine, Center for Hematology and Regenerative Medicine, Karolinska Institutet, Karolinska University Hospital, Huddinge, Stockholm, Sweden

*These authors contributed equally to this work

First published online 5 July 2020
doi: 10.1111/bjh.16868

References

1. Ucar K. Clinical presentation and management of hemolytic anemias. *Oncology (Williston Park)*. 2002;**16**:163–70.
2. Risinger M, Emberesh M, Kalfa TA. Rare hereditary hemolytic anemias: diagnostic approach and considerations in management. *Hematol Oncol Clin North Am*. 2019;**33**:373–92.
3. Kim Y, Park J, Kim M. Diagnostic approaches for inherited hemolytic anemia in the genetic era. *Blood Res*. 2017;**52**:84–94.
4. Glogowska E, Schneider ER, Maksimova Y, Schulz VP, Lezon-Geyda K, Wu J, et al. Novel mechanisms of PIEZO1 dysfunction in hereditary xerocytosis. *Blood*. 2017;**130**:1845–56.
5. Di Resta C, Galbiati S, Carrera P, Ferrari M. Next-generation sequencing approach for the diagnosis of human diseases: open challenges and new opportunities. *EJIFCC*. 2018;**29**:4–14.
6. Da Costa L, Suner L, Galimand J, Bonnel A, Pascreau T, Couque N, et al., Society of, H., Pediatric Immunology, g. & French Society of, H. Diagnostic tool for red blood cell membrane disorders: Assessment of a new generation ektacytometer. *Blood Cells Mol Dis*. 2016;**56**:9–22.
7. Johnson RM, Ravindranath Y. Osmotic scan ektacytometry in clinical diagnosis. *J Pediatr Hematol Oncol*. 1996;**18**:122–9.
8. Nichols JA, Herbert Chan HW, Baker MAB. Machine learning: applications of artificial intelligence to imaging and diagnosis. *Biophys Rev*. 2019;**11**:111–8.
9. Moura PL, Hawley BR, Mankelow TJ, Griffiths RE, Dobbe JGG, Streekstra GJ, et al. Non-muscle myosin II drives vesicle loss during human reticulocyte maturation. *Haematologica*. 2018;**103**:1997–2007.
10. Pedregosa F, Varoquaux G, Gramfort A, Michel V, Thirion B, Grisel O, et al. Scikit-learn: machine learning in python. *J Machine Learn Res*. 2011;**12**:2825–30.
11. Moura PL, Hawley BR, Dobbe JGG, Streekstra GJ, Rab MAE, Bianchi P, et al. PIEZO1 gain-of-function mutations delay reticulocyte maturation in hereditary xerocytosis. *Haematologica*. 2020;**105**: 6:e268–e271.
12. Danise P, Amendola G, Nobili B, Perrotta S, Miraglia Del Giudice E, Matarese SM, et al. Flow-cytometric analysis of erythrocytes and reticulocytes in congenital dyserythropoietic anaemia type II (CDA II): value in differential diagnosis with hereditary spherocytosis. *Clin Lab Haematol*. 2001;**23**:7–13.
13. Fermo E, Vercellati C, Marcello AP, Zaninoni A, van Wijk R, Mirra N, et al. Hereditary Xerocytosis due to Mutations in PIEZO1 Gene Associated with Heterozygous Pyruvate Kinase Deficiency and Beta-Thalassemia Trait in Two Unrelated Families. *Case Rep Hematol*. 2017;**2017**:2769570.
14. Llaudet-Planas E, Vives-Corrons JL, Rizzuto V, Gomez-Ramirez P, Sevilla Navarro J, Coll Sibina MT, et al. Osmotic gradient ektacytometry: A

valuable screening test for hereditary spherocytosis and other red blood cell membrane disorders. *Int J Lab Hematol*. 2018;**40**:94–102.
15. Zaninoni A, Fermo E, Vercellati C, Consonni D, Marcello AP, Zanella A, et al. Use of Laser Assisted Optical Rotational Cell Analyzer (LoRRca MaxSis) in the Diagnosis of RBC Membrane Disorders, Enzyme Defects, and Congenital Dyserythropoietic Anemias: A Monocentric Study on 202 Patients. *Front Physiol*. 2018;**9**:451.

Holding on to the Matutes score while dropping FMC7: new opportunity from standardised approaches in multiparameter flow cytometry

Despite significant progress in cytogenetics and molecular biology, morphology and immunophenotype remain the 'gold standard' for the diagnosis of mature B-cell lymphoproliferative disorders (B-LPD).[1] Chronic lymphocytic leukemia (CLL) represents the most frequent form of B-LPD and considering its specific phenotype, the British group from the Royal Marsden Hospital proposed in 1994 a scoring system based on the expression of five membrane markers, including FMC7, the Matutes score.[2,3] Other markers have been shown to contribute to the differential diagnosis between CLL and other CD5+ B-LPD: CD43, CD200 and more recently ROR-1.[4,5] With the development of multiparameter flow cytometry (MFC), new and wider panels for accurate diagnosis of B-LPD have been suggested. Cooperative groups like the EuroFlow consortium[5] or the ERIC & ESCCA harmonization cooperative project[4] did not select FMC7 as a required marker for CLL differential diagnosis in order to avoid redundancy and reduce the number of analyzed tubes. As FMC7 has been shown to be an epitope of CD20, both antibodies show mutual inhibition and should not be mixed in the same tube, requiring a specific tube to analyze FMC7 expression.[6]

According to sales figures from the public reagents market (personal and confidential data), one volume of the FMC7 antibody is sold for 1·38 volume of CD23, confirming that despite the addition of new markers in B-LPD panels, FMC7 was not suppressed and that Matutes score is still strongly implemented in practice. At a time when our cytometers are rising from eight to 10 to 12–13 colours, allowing combination of more informative antigens and limitation of redundancy between tubes, we have wondered if we could keep using the Matutes score replacing the FMC7 percentage (FMC7%) by the expression of CD20. This question has already been raised by others, with conflicting results,[7,8] but that was before the implementation of standardised operating procedures (SOP) in flow laboratories.[9] In the present work, we investigated the value of using CD20 expression instead of FMC7% in the Matutes score for CLL diagnosis in a context of SOP for multiparameter flow cytometry.

A cohort of 508 patients with B-LPD issued from two centres (Ambroise Paré and Saint Louis, Paris, France) was included in this multicentre retrospective study. All blood samples were immunophenotyped according to EuroFlow SOP within the FranceFlow Quality Assessment Programme for the Lymphoid Screening Tube (LST) tube[10] and to local procedures for the tube including FMC7, using eight-colour immunophenotyping panels on Canto II (BD Biosciences, San Jose, CA, USA; $n = 458$) and Lyric (BD Biosciences; $n = 50$) flow cytometers. Morphological, immunophenotypic, cytogenetic and molecular analyses, as well as clinical data, were collected to establish consensual integrated diagnoses according to the criteria of the World Health Organization (WHO) classification.[1] Matutes score was calculated as previously published.[3] All analyses were performed using Stata Statistical Software: release 14 (Stata Corp., LLC, College Station, TX, USA). Correlation matrix was performed using the R Corrplot package (R Foundation for Statistical Computing, Vienna, Austria). The clinical and biological characteristics of the study population are reported in Tables SI and SII, and Fig S1.

We first analysed the correlation between CD20 expression, CD20 mean fluorescence intensity (MFI), FMC7%, FMC7 MFI and FMC7 ratio, i.e. the MFI of B cells normalised to the MFI of non-B lymphocytes, as cytometers were not harmonised for this parameter contrary to CD20. Overall, the best correlation was found between CD20 MFI and FMC7% ($\rho = 0{\cdot}620$, $P < 10^{-4}$), FMC7 MFI and FMC7 ratio showed lower correlations with CD20 MFI ($\rho = 0{\cdot}462$ and $\rho = 0{\cdot}472$, $P < 10^{-4}$, respectively) Fig 1A. Using receiver operating characteristic (ROC) curves we compared the diagnostic performance of CD20 MFI, FMC7%, FMC7 MFI and FMC7 ratio. Surprisingly, CD20 MFI showed the highest diagnostic performance. Using the Youden index, the discriminating CD20 MFI threshold was defined as 6000. With this cut-off, the sensitivity for the diagnosis of CLL was 84·7% and specificity 94·9% (Fig 1B), the positive predictive value (PPV) and negative predictive value (NPV) were 95·1% and 84·1%, respectively. Using the classical FMC7